ARTICLE IN PRESS

Communications Biology

https://doi.org/10.1038/s42003-026-09881-8

Article in Press

Evolutionary history of Chinese cavefishes parallels paleogeoclimatic and river capture processes

Received: 30 June 2025

Accepted: 6 March 2026

Cite this article as: Luo, T., Xiao, M.-Y., Liao, M. *et al.* Evolutionary history of Chinese cavefishes parallels paleogeoclimatic and river capture processes. *Commun Biol* (2026). https://doi.org/10.1038/s42003-026-09881-8

Tao Luo, Ming-Yuan Xiao, Mei Liao, Jia-Jia Wang, Ning Xiao & Jiang Zhou

We are providing an unedited version of this manuscript to give early access to its findings. Before final publication, the manuscript will undergo further editing. Please note there may be errors present which affect the content, and all legal disclaimers apply.

If this paper is publishing under a Transparent Peer Review model then Peer Review reports will publish with the final article.

ARTICLE IN PRESS

© The Author(s) 2026. **Open Access** This article is licensed under a Creative Commons Attribution-NonCommercial-NoDerivatives 4.0 International License, which permits any non-commercial use, sharing, distribution and reproduction in any medium or format, as long as you give appropriate credit to the original author(s) and the source, provide a link to the Creative Commons licence, and indicate if you modified the licensed material. You do not have permission under this licence to share adapted material derived from this article or parts of it. The images or other third party material in this article are included in the article's Creative Commons licence, unless indicated otherwise in a credit line to the material. If material is not included in the article's Creative Commons licence and your intended use is not permitted by statutory regulation or exceeds the permitted use, you will need to obtain permission directly from the copyright holder. To view a copy of this licence, visit http://creativecommons.org/licenses/by-nc-nd/4.0/.

Evolutionary history of Chinese cavefishes parallels paleogeoclimatic and river capture processes

Tao Luo[1,2,5], Ming-Yuan Xiao[3], Mei Liao[1], Jia-Jia Wang[1], Ning Xiao[4], Jiang Zhou[1*]

[1] School of Karst Science, Guizhou Normal University, Guiyang, China

[2] School of Life Sciences, Yunnan University, Kunming, China

[3] School of Life Sciences, Guizhou Normal University, Guiyang, China

[4] Guiyang Healthcare Vocational University, Guiyang, China

[5] Southwest United Graduate School, Kunming, China

*Corresponding authors. E-mail: zhoujiang@ioz.ac.cn

Abstract

The karst ecosystem in southwestern China is a global hotspot for cavefish diversity research, yet the origins and evolutionary history of this diversity remain poorly understood. To elucidate their evolutionary origins and history, we analyzed 183 cavefish species and their close relatives from ten clades. Our findings indicate that freshwater fishes began colonizing caves ~44 million years ago (Ma). Speciation was driven by in situ diversification, starting around 43.2 Ma, increasing sharply by ~35 Ma and 18 Ma, and peaking at ~8.3 Ma, 2.5 Ma, and 1.5 Ma. Distinct hydrological basins exhibited divergent diversification patterns. Dispersal between the Pearl and Yangtze River basins began by ~24.1 Ma, accelerated around 21 Ma, 13 Ma, and 9.6 Ma, and peaked at ~13 Ma, 5 Ma, and 2 Ma. We propose that river drainages in southwestern China developed stepwise from the late Eocene to early Pleistocene, with connectivity between the Pearl and Yangtze basins established by the late Oligocene (~26 Ma). The origin and diversification of cavefishes are closely linked to the evolution of karst landscapes, shaped by orogeny and monsoon-driven climate changes since the late Eocene. These insights are crucial for informing conservation strategies for these unique habitats under ongoing climate change.

Keywords: biogeography, evolution, biodiversity, *in situ* diversification, speciation

Introduction

The evolution of natural landscapes in Asia is closely linked to geotectonic processes and paleoclimatic changes[1]. The current consensus is that the Indian–Eurasian collision during the Cenozoic resulted in the uplift of the Qinghai–Tibet Plateau (QTP)[2,3], an event that fundamentally altered the region's geomorphology[1] and shaped the evolutionary trajectory of species across Asia[4,5]. Following the formation of the QTP, subsequent orogenic events further influenced the development of major drainages and contributed to the reorganization of East Asia's paleoclimate[6]. These geological processes were instrumental in the origin of the Yangtze River[7] and the Pearl River[8], the Asian monsoon[2,6], and the diversification of regional biota[5,9,10]. Under the combined influence of paleogeological and climatic conditions, subterranean ecosystems underwent substantial transformations[11], playing a pivotal role in shaping and preserving regional biodiversity[12,13]. However, a comprehensive understanding of the spatiotemporal evolution of Asian cave systems and their impact on the diversity of subterranean biota remains elusive, primarily due to the limited extent of current research.

The geologic processes shaping natural landscapes and their influence on evolutionary processes have profoundly influenced the diversification of the extant biota[14-17], a concept now widely accepted in biogeography[18,19]. As such, reconstructing the phylogeography of diverse extant species can provide valuable insights into geological evolution[18,19]. Caves can be considered as subterranean ecological islands with distinct characteristics, interconnected with surface environments through rivers or karst aquifers[20], and paleogeoclimatic events have strongly influenced cave biodiversity[12]. Among vertebrates, the cavefishes are exemplary species exhibiting unique adaptations to subterranean life, the most notable being the degeneration or absence of pigmentation, eyes, and scales[21]. Based on their differential dependence on cave environments, cavefishes are divided into two ecological types: troglomorphic (typical, stygobionts) and non-troglomorphic (atypical, stygophiles)[22,23]; a dichotomous classification scheme adopted here. Cavefishes are obligate freshwater inhabitants of caves, and closely related species are often found in surface waters. Consequently, the biogeographic dynamics of cavefishes can, in theory, be reconstructed as a response to the historical processes of cave formation and evolution. However, current studies on the biogeographic patterns of cavefishes are frequently limited to single taxa[13,24,25]. In the context of global warming, potential droughts and diminished groundwater recharge in caves may irreversibly impact cavefish populations[26,27], underscoring the critical need to advance our understanding of subterranean biodiversity and its evolutionary origins.

In China, cavefishes are primarily documented in the southwestern region, particularly in the karst areas of the upper Pearl River (including the Beipanjiang, Guijiang–Hejiang, Hongshui, Zuojiang–Youjiang, and Liujiang rivers), the upper Yangtze River (encompassing the Jinshajiang, Wujiang, and Yuanjiang rivers), and the Red River Basin[28]. However, despite being recognized as a biodiversity hotspot and conservation priority, the diversity of these subterranean fishes remains severely underestimated due to insufficient field surveys and systematic research, and their evolutionary history remains poorly understood. Although several studies based on incomplete sampling and reduced-representation genomic data have revealed the important roles of paleoclimatic history and gene flow in driving the speciation and radiation of *Sinocyclocheilus*[29], their limited taxonomic scope still precludes a comprehensive understanding of the evolutionary history of Chinese cavefishes and the associated geomorphological evolution—such as river formation and connectivity. Furthermore, it remains unclear whether historically warm climates in geological time promoted diversification bursts or had the opposite effect. Therefore, integrated evolutionary analyses of multiple cavefish clades will help predict their response trajectories under global warming and inform adaptive conservation strategies and interventions.

In this study, we compiled a species list of Chinese cavefishes and reconstructed the most extensive phylogeny to date, comprising 208 species in ten phylogenetic trees, representing two orders, six families, and 22 genera. We employed fossil-based and secondary calibration methods to estimate the origin and divergence times of cavefishes (see the Supplementary Note 1 for details), and further assessed their diversification history. Combining this evidence with the distribution of species sheds light on the origin and diversification dynamics of Chinese cavefishes, as well as the history of connectivity between the Pearl and Yangtze Rivers.

Results

Biodiversity hotspots of Chinese cavefishes

A literature search obtained data for ~199 species of cavefishes in China described as of October 31, 2025 (Supplementary Data 1). Eastern Yunnan, southern Guizhou, and northwestern Guangxi, provinces in the karst region of southwestern China, were identified as biodiversity hotspots for cavefishes in Asian (Fig. 1A). In these regions, species richness exceeded eight species per grid cell. We also employed records from the upper Yangtze River, India, and Indochina (Fig. 1A).

Biogeographic events and the corresponding relative ages

Although a comprehensive list of ~199 species was initially compiled, practical constraints ultimately led us to employ ten independent time-calibrated phylogenies, encompassing 183 species and their close relatives, to investigate the diversification of Chinese cavefishes (Figs. 2 and Supplementary Fig. 1–10; Supplementary Tables 2–8; Supplementary Data 2–4). An ancestral habitat and region reconstruction using these ten time-calibrated phylogenies revealed 376 events associated with the speciation and diversification of cavefishes (Supplementary Figs. 11–23). These comprised 49 dispersal events (13.0%), 307 *in situ* diversification events (81.7%), 20 instances of migration into caves (5.3%), and two instances of migration outside of caves (Supplementary Tables 9–11; Supplementary Data 5). The respective mean times of occurrence for these events were 10.0 million years ago (Ma) (95% CI = 12.3–8.0), 8.0 Ma (95% CI = 8.9–7.2), 20.9 Ma (95% CI = 27.8–14.7), and 19.9 Ma (95% CI = 20.6–19.3) (Table 1). There was a notable clustering of events around ~10 Ma, particularly between the Pearl River and the Yangtze River (Table 1). This dense concentration of diversification events in the late Miocene suggests the occurrence of distinct paleogeoclimatic events in southwest China during this period.

Dynamics of diversification events through time

The dynamics of *in situ* diversification, dispersal, and lineage divergence rates have remained relatively stable over time under most biogeographic models. The ancestors of Chinese cavefishes began to enter caves as early as the late Paleocene (~44 Ma), with colonization accelerating ~42 Ma and 9 Ma, and peaking at ~32 Ma, 26 Ma, and 13 Ma (Supplementary Fig. 24A, Supplementary Table 12). Dispersal, *in situ* diversification, and lineage divergence events associated with Chinese cavefishes occurred ~33 Ma, 43 Ma, and 39 Ma, respectively (Fig. 3A, Supplementary Data 5). The rates of *in situ* diversification, dispersal, and lineage divergence remained relatively low, gradually increasing from ~45 to 35 Ma. Starting at ~35 Ma, the rate of in situ diversification increased sharply, accelerated further around 18 Ma, reached its first peak at ~8.3 Ma before declining to a valley at ~3.4 Ma, then rose to a second peak at ~2.5 Ma followed by a third peak at ~1.45 Ma and a subsequent rapid decrease (Fig. 3A; Supplementary Table 12). Dispersal events gradually increased from ~34 to 4.5 Ma, accelerated around 23.5 Ma, 14.2 Ma, and 4.2 Ma, and peaked at ~16 Ma, 5.9 Ma, and 4.4 Ma. Distinct valleys occurred at around 17.6 Ma, 8.2 Ma, and 13.8 Ma, followed by a rapid decline after ~4 Ma. Lineage divergence, starting from ~39.5 Ma, accelerated around 35.6 Ma and 15.1 Ma, reached peaks at approximately 9.0 Ma, 2.48 Ma, and 1.4 Ma, with corresponding valleys at about 24.7 Ma, 13.6 Ma, and 3.4 Ma, and decreased rapidly after ~1 Ma (Fig. 3A; Supplementary Table 12). Overall, these patterns indicate a gradual increase in diversification from the late Eocene to the Pleistocene. The dynamics of diversification align with both the Stepwise and Late-uplift hypotheses regarding the origin of the QTP (Fig. 3G).

We also assessed the *in situ* diversification of cavefishes across ten river drainages, whose geological locations are shown in Figure 1B. The maximum number of observed *in situ* diversification events per 0.3 million years (MDivE) revealed an asynchronous pattern (Fig. 3B). Diversification events in the drainages of the Guijiang–Hejiang, Nanpanjiang, Zuojiang-Youjiang, Hongshui, and Liujiang Rivers began during the late Eocene to mid-Oligocene (~39 to 27 Ma); these were followed by the Miocene drainages of the Wujiang, Yuanjiang, Jinshajiang, and Panlongjiang Rivers (~22 to 11 Ma) (Supplementary Table 13). *In situ* diversification in the Beipanjiang River occurred last, during the late Oligocene (~9 Ma) (Fig. 3B, Supplementary Table 13). The Nanpanjiang, Hongshui, and Liujiang rivers display distinct temporal patterns in their evolutionary histories: the Nanpanjiang River is characterized by three peaks (at ~22 Ma, 8.8 Ma and 4.1 Ma) and two valley (at ~18.3 Ma and 7.1 Ma); the Hongshui River exhibits three prominent peaks (at ~26.0 Ma, 16.5 Ma, and 2.5 Ma) and two valleys (at ~21.6 Ma and 13.8 Ma); while the Liujiang River shows four peaks (at ~13.4 Ma, 9.5 Ma, 5.0 Ma, and 0.9 Ma) and three valleys (at ~12.5 Ma, 7.6 Ma, and 3.9 Ma) (Fig. 3B). In contrast, the remaining rivers are marked by a single prominent peak occurring between ~11.0 Ma and 4.0 Ma (Fig. 3B).

Biotic interchange between the Pearl and Yangtze Rivers

The ancestors of cavefishes from the karst region of southern China were likely to have inhabited the paleo-Pearl River (Supplementary Figs. 21–23). The dispersal of cavefishes from the Pearl River to the Yangtze River occurred around ~24.1 Ma (95% CI: 26.1–17.4), earlier than the dispersal from the Yangtze River to the Pearl River, which occurred ~13.0 Ma (95% CI: 13.5–10.0) (Fig. 3C, Supplementary Tables 12 and 14). Both dispersal events accelerated at ~21.7 Ma, ~13.2 Ma and 9.6 Ma (Supplementary Fig. 24O and 24P, Supplementary Table 12), and peaked at ~13 Ma, 2 Ma, and 5 Ma, respectively (Fig. 3C, Supplementary Table 12). Overall, the patterns of cavefish interchange between the two river systems were broadly similar yet intermittent, particularly for the dispersal from the Yangtze River to the Pearl River (Fig. 3C). This intermittency suggests that hydrological connectivity between these major rivers was likely dynamic, appearing and disappearing multiple times over their geological history.

Discussion

The diversification of Chinese cavefishes is closely linked to orogeny and the creation of the monsoon climate. The diversification curves for the maximum number of observed migration events into caves per 0.3 million years (MCE), the lineage divergence events per 0.3 million years (MDE), and dispersal events per 0.3 million years (MDisE) indicate that Chinese freshwater fishes first entered caves during the middle Eocene (~44 Ma). *In situ* diversification, lineage divergence, and dispersal began near the middle Eocene to Eocene–Oligocene boundary (~44–33 Ma), with rates accelerating at ~35, 15, and 23 Ma, and a marked increase occurred ~35 Ma (Fig. 3A, Supplementary Table 12). These times align with key orogeny events in Asia, such as the India–Asia hard collision (~45 Ma)[30,31], rapid uplift along the eastern margin of the QTP (~45–35 Ma, Fig. 3D)[2], left-lateral extrusion of Indochina started ~35Ma[32-35], and the rapid uplift of the QTP (~25–15 Ma, Fig. 3D)[2]. Concurrent with these orogenic events, the Youjiang region, Gunagxi—a hotspot for Chinese cavefishes (Fig. 1A)—developed a series of NW-trending fault zones and associated basins through left-lateral strike-slip motion during the Cenozoic[36,37] (Fig. 1C). This tectonic framework likely provided potential pathways for the early ancestors of cavefishes to colonize subterranean habitats and facilitated subsequent karst erosion processes. The dramatic decline in global temperatures at the Eocene–Oligocene boundary (~34 Ma) may have catalyzed the initial cave colonization and subsequent subterranean adaptation of cavefish ancestors[38,39]. During this process, their ancestors innovatively evolved specialized morphological and genetic functions, exemplified by the regression of energy-consuming organs (e.g., eyes, scale, and pigmentation)[29,40], enhancement of energy-storage and sensory organs (e.g., the caudal adipose keel and the distinctive horns or humps in some cave-adapted *Sinocyclocheilus* species)[29,40,41], and unique genetic regulatory mechanisms[42,43]. This hypothesis is chronologically consistent with the estimated timing of cave colonization (Figs. 3A and 4), and may have preceded the emergence of *in situ* speciation (Fig. 4). In addition, palaeobotanical fossils and paleoclimatic evidence suggest that the establishment of the East Asian summer monsoon during the late Oligocene (~25 Ma) brought substantial rainfall [44-46], a period which coincides with and may have accelerated the observed pulses of *in situ* diversification and lineage divergence at ~25 Ma (Fig. 3A). From 25 to 5 Ma, the MDivE, MDisE, and MDE curves increased almost linearly, with MDivE and MDE showing four smaller phases: 25–21, 21–13, 13–4, and 4–2.5 Ma (Fig. 3A). These phases essentially correspond to the rapid uplift of the QTP (25–15 Ma, 5.3–2.5 Ma)[2,47] (Fig. 4) and the extrusion of Indochina (35–16 Ma, 11–5 Ma)[32,35,48,49]. Furthermore, the increased intensity of the East Asian monsoon from ~15 to 4 Ma likely contributed to the rapid radiation of cavefishes[50,51] (Fig. 4). Despite global temperatures experiencing a shift from cool to colder periods [39] from 25 to 2 Ma, recent climate simulations suggest that southwestern China experienced relatively stable temperatures in the range of ~16–20°C or even experienced a slight increase[1]. The combined effects of ongoing orogeny, intensified monsoon rainfall, and relatively stable regional climates likely created conditions conducive to accelerated karst erosion and cave formation[11,52]. These processes, in turn, may have facilitated the observed burst in in situ speciation of cavefishes (Fig. 4). Although the specific influences of cave and groundwater on cavefish diversification cannot be precisely reconstructed at present, their role in shaping dispersal, *in situ* diversification, and distribution patterns should not be underestimated.

In situ diversification dynamics of Chinese cavefishes show a close correspondence with phased karst development. Our MDivE analysis revealed three accelerated phases of cavefish diversification: ~35–25 Ma, 25–4 Ma, and from 4 Ma to the present. These phases broadly correspond to the three previously proposed phases of karst formation in southern China based on geological evidence: S1 (~66–23 Ma), S2 (~23–2.5 Ma), and S3 (~2.5 Ma–present)[11]. These phases occurred to varying degrees across Yunnan, Guangxi, and Guizhou Provinces in southwestern China[11]. During the S1 phase, isolated lake basins formed as a result of the late Cretaceous to the late Paleocene orogeny, and many more lakes were created by the continued orogeny. However, numerous cave ecosystems and underground rivers had not yet appeared[11]. The relatively stable geological movements during this phase align with the gradual increases in MDivE, MDisE, and MDE observed between ~35 and 25 Ma (Fig. 3A). During this period, the ancestors of the cavefish began to be isolated into multiple small ancestral populations, and *in situ* speciation emerged (Fig. 4). During the S2 phase, the Darong movement in Guangxi accelerated uplift in the western regions, prompting rivers to shift from west to east and marking the end of the lake basin era[11]. This phase was also characterized by intense orogeny[2,32,48,53,54], a relatively warm and humid climate[1], and increased monsoon rainfall[10,45,46,50]—conditions considered favorable for the development of karst cave environments[1]. The MDivE, MDisE, and MDE analyses support a potential link between the accelerated diversification from 25 to 4 Ma and the rapid formation of S2-phase karst caves. This period of extensive karstification coincides with and may have facilitated the observed *in situ* speciation burst (Figs. 3A and 4). Entering the S3 phase, i.e., the Pleistocene, the key features included the formation of East Asian landscapes[1], a weakening of orogeny[1,2,35], decreased CO_2 levels (Fig. 3E)[1,55], and a decline in global temperatures and monsoon rainfall due to the onset of the glacial period (Fig. 3F) [1,39,50]. These factors may have contributed to a deceleration in karst cave formation. This slowdown coincides with a gradual decline in diversification rates after ~5 Ma (Fig. 3A), suggesting a potential linkage. In other words, while long-term global temperature rise could theoretically promote cavefish diversification under idealized conditions, the current degradation of subterranean ecosystems and the need to balance conservation with sustainable human benefits render *in situ* protection of cavefishes urgently needed. Integrating our three-phase MDivE model with current geological evidence[11,56], we suggest a revised timeline for karst formation in southwestern China: (1) from the Paleocene to the late Oligocene (~66–25 Ma); (2) from the late Oligocene to the early Pliocene (~25–5 Ma); (3) from the Pliocene to the current (~5 Ma–present)[56]. This revision shifts the onset of the final stage forward by at least 2.5 Ma, placing its initiation in the Pliocene rather than the Pleistocene. The updated chronology aligns with recent evolutionary biogeographic studies in the region[12,35,57]. However, given the unique climatic conditions of the Pleistocene and the presence of glacial refugia in southern China, the S3 phase may be further subdivided into two substages—5 to 2.5 Ma and 2.5 Ma to present—to better reflect the diversification patterns and demographic histories observed across different regions and taxa[12,29,35,57].

The evolution of Chinese cavefishes aligns with both the Stepwise Hypothesis[58] and the Late Orogeny Hypothesis[47], as well as with models that have recently been proposed to explain the uplift of the QTP (Fig. 3G). The temporal progression of these geological events coincides with the early and late stages of cavefish diversification, including the origin in the Paleocene (with the origin of the genus *Horaglanis* in India between 69.26 and 53.92 Ma, Supplementary Fig. 8), the initial acceleration during the Miocene, and the peak in the late Pliocene (Fig. 3A, Supplementary Table 12). Thus, for biota located far from the QTP orogenic belt, integrating both hypotheses may provide a comprehensive framework for explaining their historical diversification. The diversification curve accelerated slightly during each phase, consistent with a model of cave formation in southwest China that was non-uniform or episodic.

Finally, although our study reveals a coupling between paleoclimatic changes and bursts of cavefish diversification, incomplete sampling of both cave-adapted and surface-dwelling relatives, and extinction of surface lineages may influence the robustness of these findings. Additionally, the contribution of genetic factors such as gene flow to cavefish diversification remains incompletely understood—a key limitation of this work. For instance, previous studies have demonstrated that gene flow facilitated adaptive radiations in primates[59,60], voles[61], bats[62], QTP fishes[63], and cichlids[64]. While phylogenomic analyses of *Sinocyclocheilus*[29] have revealed how gene flow and paleoclimatic shifts jointly promoted its radiation, it remains unclear whether similar mechanisms operate in other cavefish groups or what genomic features characterize introgressed regions. Thus, future phylogenomic studies encompassing broader taxonomic groups will be essential to advance understanding of the origins, diversification bursts, and adaptive radiation of the cavefish hotspot in the karst regions of southwestern China.

Phylogenetic evidence supports the stepwise formation of river drainages in southwestern China. The diversification patterns of cavefishes exhibit a strong temporal correlation with this asynchronous river development. Our MDivE analysis supports the hypothesis that the *in situ* diversification of cavefishes originated at different times across various drainages (Fig. 3B). MDivE analyses of the Hongshui, Guijiang–Hejiang, Nanpanjiang, Zuojiang–Youjiang, and Liujiang rivers indicate that the *in situ* diversification of Chinese cavefishes originated at 39.9 (95% CI: 40.8–31.5), 37.4 (95% CI: 45.0–12.9), 33.6 (95% CI: 33.3–31.2), 33.3 (95% CI: 34.20–23.40), and 27.6 (95% CI: 29.1–23.9) Ma, respectively, with accelerated rates occurring between 28 and 8 Ma (Fig. 3B and Supplementary Table 13). This suggests that these river systems in the Pearl River Basin likely originated during the late Eocene to Oligocene, with accelerated formation occurring from the late Oligocene to middle Miocene[65]. These patterns correspond to the accelerated left-lateral extrusion of the Indochina (35–16 Ma)[32-35,66], the rapid uplift of the QTP (25–15 Ma)[2], and intensified monsoon events in the Zuojiang-Youjiang[45,46], as indicated by geological evidence. During this period, the southeastern extrusion of Indochina was estimated to cover at least 500 km at a rate of 4 to 5 cm/year[32,48,49], sufficient to cover the entire extant distribution of the Chinese cavefishes (Fig. 1), and the timing coincided with the extent of river drainages, especially the Nanpanjiang River. From 16 to 8 Ma, the MDivE of the Nanpanjiang River, Liujiang River, and Zuojiang-Youjiang River increased sharply, peaking at ~9.5 Ma, aligning with the right-lateral extrusion of Indochina[35,67,68], maximum Asian Monsoon intensification[50,69], faster erosion of landforms[52,69] during the late Miocene. This extrusion occurred at an average rate of 5 mm/year over at least 25 km[70]. Thermochronological data (8.4–6.8 Ma) from the Ailao Shan region further support this hypothesis [68]. The combined effects of the right-lateral extrusion of Indochina (11–5 Ma) [67,68,70] and the intensification of the East Asian monsoon (15–4 Ma) [50] may have facilitated the formation of several other rivers, including the Jinshajiang (~12 Ma), Panlongjiang (~12 Ma), Yuanjiang (~11 Ma), and Beipanjiang (~9 Ma). The MDivE of the Hongshui River originated at 39.9 Ma (95% CI: 40.8–31.5) and accelerated at 16.9 Ma (95% CI: 19.39–14.47), consistent with geological evidence indicating that the river itself originated during the late Eocene-early Oligocene[65] and underwent rapid formation in the Late Oligocene[8]. Similarly, the MDivE for the upper Yangtze-Wujiang River at ~22.4 Ma (95% CI: 27.6–13.2) aligns with geological evidence, indicating that the modern Yangtze River formed during the late Oligocene and early Miocene[7,71,72]. Additionally, the first distinct peak in MDivE across 90% of the river basins occurred between 11 and 5 Ma (Fig. 3B), consistent with geological evidence indicating rapid karst landscape development driven by the combined effects of orogeny[67,68,70], Asian monsoon intensification[50,69], and favorable climatic conditions. This period aligns with the key stages of karst evolution in southern China, i.e., according to the classical model of geomorphic evolution, this region sequentially experienced the Mountain-Basin Stage, the Planation Period, the Fenglin Stage, and the Shilin Stage[11]. The MDivE peaks of the Nanpanjiang, Hongshui, upper Yangtze-Wujiang, Beipanjiang, and Jinshajiang rivers, dated to ~5.0–1.0 Ma, correspond to the Nanpanjiang, Hongshui, and Wujiang–Jialingjiang stages of karst evolution in the S3 phase [11].

These findings suggest that our dynamic meta-analysis, based on the biogeography of multiple taxa, is a plausible model for understanding the formation of drainages in southwestern China. We observed multiple distinct inflection points in the MDivE curve (Supplementary Table 13), indicating that the formation of these drainages involved several distinct acceleration events rather than being a uniform process. Based on phylogenetic evidence, we propose a five-step hypothesis for the formation of these drainages in southwestern China: (1) from the middle to late Eocene (~45–35 Ma); (2) from the late Eocene to the late Oligocene (~35–25 Ma); (3) from the late Oligocene to the early Miocene (~25–18 Ma); (4) from the early to late Miocene (~18–7 Ma); and (5) from the Pliocene to the present (~5–0 Ma). This hypothesis contrasts with geologic models that suggest that the Pearl River basin began to develop in the late Oligocene[8] or Miocene[65]. The asynchronous and non-uniform nature of river formation in southwestern China is likely a far-field response to paleo-geoclimatic events driven by the Indo-Asian collision. Nevertheless, our proposed stepwise river formation hypothesis may be influenced by limited data, possibly explaining the partial mismatch between in situ diversification peaks in Figure 3C and those in Supplementary Table 13. Future studies with more comprehensive data could help substantiate this hypothesis.

Biological evidence suggests a historical connection between the Yangtze and Pearl Rivers, which may have become linked as early as the late Oligocene. Geological studies place the formation age of the present-day Yangtze River system to ~36.5–23.0 Ma[7] or late Miocene[71], with the first bend occurring ~35 Ma[72]. Conversely, the origin of the Pearl River dates to the late Oligocene, 27–23 Ma[8], with the modern drainage basin pattern beginning to develop in the mid-Miocene, around 16.0–13.8 Ma[65]. Our MDisE analysis indicated that dispersal from the Pearl River to the Yangtze River commenced around ~24.1 Ma (95% CI: 26.10–17.4) and persisted until ~1.0 Ma (Fig. 3C), while reverse dispersal from the Yangtze to the Pearl River began at ~13.0 Ma (95% CI: 13.50–10.0) and continued until ~0.5 Ma. These results suggest that ancestral populations of cavefishes from the Paleo-Pearl River dispersed into the Paleo-Yangtze River as late as the late Oligocene, providing further evidence that by the Oligocene–Miocene boundary (~23 Ma), the modern Yangtze River had not yet formed[73] and the Paleo-Jinshajiang likely flowed southward into a river analogous to the modern Nanpanjiang River. This hypothesis of a southward-flowing Paleo-Jinshajiang River, supported by zircon U–Pb dating[72,74], posits that prior to substantial QTP uplift, this river drained into the South China Sea. Subsequently, between ~35 and 28 Ma, the river is inferred to have shifted northeastward[72]—an event known as the Paleo-Jinshajiang diversion—forming the upper reaches of the modern Yangtze River. This earlier river system was ultimately eliminated by the QTP uplift between ~23 and 15 Ma[72,74]. Independent biogeographic evidence also indicates dispersal of East Asian cyprinids from the Pearl River to the Yangtze River at ~23 Ma, with reverse dispersal occurring as early as ~15 Ma[73]. Our results are therefore consistent with evidence from both geology and biogeography. Collectively, these independent lines of evidence converge to suggest that the Yangtze and Pearl Rivers were likely connected by at least the Oligocene–Miocene boundary.

Asynchronous dispersal patterns observed between the Pearl and Yangtze River basins are temporally associated with differences in the formation timelines of their subterranean river–lake complex ecosystems. This phase corresponds temporally with the rapid uplift of the QTP (25–15 Ma)[2] and left-lateral extrusion of Indochina (35–16 Ma)[32-35], with dispersal rates declining as these orogenic events waned—a pattern consistent with the stepwise uplift hypothesis of the QTP[58]. In contrast, dispersal from the Yangtze to the Pearl accelerated during 14–4 Ma, peaking at ~5.0 Ma, and subsequently declined (Fig. 3C). This later phase aligns with Middle Pliocene uplift of the QTP[47] and intensification of the Asian monsoon (~15–4 Ma)[50,69]. An asymmetric dispersal peak from the Pearl to the Yangtze was also observed at ~2 Ma. We hypothesize that repeated, short-lived connections between adjacent subterranean rivers—later rapidly disrupted—may have limited dispersal into the Pearl River basin. This is exemplified by the *Sinocyclocheilus multipunctatus* complex, distributed across both basins but exhibiting recent divergence among populations. Additionally, local orogeny along basin boundaries may have contributed to this asymmetry. For example, geological evidence suggests that the Wumeng–Miaoling Mountains, which formed during the far-field effects of the QTP orogeny[47,75], likely served as a barrier between the Pearl and Yangtze River basins in Guizhou, particularly from the Pliocene (~5.33–2.58 Ma) through the Pleistocene (~2.58 Ma). Collectively, the observed dispersal patterns suggest a strong association between cavefish dispersal across the Yangtze and Pearl River basins and major orogenic and monsoon-driven climatic events since the Miocene. These findings are consistent with the interpretation that the Pearl and Yangtze Rivers maintained well-developed subterranean river-lake ecosystems[73] during the middle Oligocene–Miocene and Middle Miocene–Pliocene, respectively. By aligning biological diversification events with independent geological timelines, our study offers a biological perspective that is consistent with and refines the estimated chronology of major geological and ecological events in the evolutionary histories of these river systems. This integrative approach advances our understanding of their development and establishes a paradigm for reconstructing subterranean aquatic ecosystems. However, the limited taxonomic representation of cavefishes across these two basins may affect the robustness of our findings. Future studies incorporating a broader range of subterranean and surface-dwelling lineages would help to test, strengthen, and extend the proposed framework.

Cavefishes are recognized as valuable models for biogeographic studies, with substantial evidence supporting their utility in revealing how paleogeographic events have shaped speciation and adaptive evolution in subterranean ecosystems[13,24,25,29,40,76]. However, investigations focused on a single taxonomic group may have limited capacity to fully reconstruct how paleoclimatic and geological processes have influenced biodiversity evolution across broader spatial and temporal scales. Our study builds upon and extends prior work in several key dimensions. For instance, a recent phylogenomic study by Mao et al.[29] provided critical insights into the roles of paleoclimate and gene flow in the radiation of the genus *Sinocyclocheilus.* While both studies document a strong association between paleoclimatic events and cavefish evolutionary history, our work expands the scope in notable ways. First, we incorporated a substantially broader taxonomic sample (183 species, representing ~92% of known extant Chinese cavefishes) by integrating newly sequenced and publicly available data, offering a more comprehensive perspective on the origins of the regional cavefish diversity hotspot. Second, while Mao et al.[29] employed reduced-representation genomic data to reveal complex gene flow patterns within *Sinocyclocheilus*, our study utilized mitochondrial markers. Multiple studies have validated the utility of mitochondrial data, particularly with comprehensive node calibration, for inferring deep diversification histories and biogeographic events[12,18,19,35,77-80]. Third, beyond shared focal drivers like QTP uplift and monsoon evolution, our analytical framework explicitly incorporated the effects of additional geophysical processes—including Indochina extrusion, phased karst development, and river capture events—and quantitatively reconstructed drainage network evolution through in situ diversification and dispersal metrics. In summary, the methodological and analytical differences between these studies provide complementary insights into the evolutionary history of Chinese cavefishes. Patterns such as cross-species gene flow identified at the genomic level may help explain biological events not fully resolved by phylogenetic methods alone[29]. Future phylogenomic studies with expanded taxon sampling across diverse cavefish lineages will be essential to integrate these perspectives and further elucidate the mechanisms of speciation and diversification in this unique fauna.

In conclusion, this study compiled data for 199 currently recognized Chinese cavefishes, identifying two major diversity hotspots. By integrating genetic data from 183 cave-adapted and related surface-dwelling species, we reconstructed a comprehensive phylogeny to explore their diversification history. To our knowledge, this represents the most taxonomically inclusive phylogenetic framework for Chinese cavefishes to date. Our analyses indicate that cave colonization likely began in the middle Eocene (~44 Ma), with in situ diversification emerging as the predominant mode of speciation. This process started around 43.2 Ma, accelerated markedly by ~35 Ma and 18 Ma, and exhibited two major peaks at ~8.3 Ma and 2.5 Ma, with a notable decline at ~3.3 Ma. Diversification patterns varied regionally across river basins, showing staggered origins and asynchronous periods of acceleration and peak periods. In summary, this work establishes a valuable spatiotemporal framework for understanding speciation and biogeography in subterranean environments, offering a compelling case study of the interplay between tectonic, climatic, and biological evolution. However, limitations such as persistent gaps in taxon sampling and the current lack of genome-scale data may affect phylogenetic resolution and obscure the role of processes like gene flow. Future studies should prioritize expanded taxonomic sampling and generate high-quality genomic resources to further elucidate the diversification history, evolutionary mechanisms, and ecological adaptations of these unique subterranean biotas.

Methods

Collection of distribution data

We compiled a catalog and distribution records of cavefishes in China and adjacent regions through long-term field surveys, a comprehensive literature review, and database searches (https://www.fishbase.de; https://www.gbif.org/). Distribution data for newly described species were obtained from Google Scholar and CNKI (https://www.cnki.net/) using the following keywords: “cave fish,” “blind fish,” and “cave-dwelling fishes”. The scientific names of each species were carefully checked to avoid potential synonyms. In total, 370 occurrence sites for 221 species were included in the analysis (Supplementary Data 1). The distribution sites for each species were rasterized to a 0.5° × 0.5° resolution (~50 km × 55 km) grid system using ArcGIS v.10.4. Species richness was determined by summing the total number of species present in each grid cell.

Taxon sampling, sequencing, and data collection

In total, 87 tissue samples from 12 genera across three families were collected in the Karst region of southwest China between 2016 and 2024. All sampling procedures were performed with ethical consideration, whereby fin clips were collected non-invasively from fish anesthetized with Tricaine (150 mg/ml) that were subsequently revived and released, or were obtained only after natural death. Genomic DNA was extracted from the muscle tissues of fish preserved in 95% anhydrous ethanol using a standard extraction kit (Vazyme Biotech, Nanjing, China). We have complied with all relevant ethical regulations for animal use.

For mitochondrial genome sequencing, library preparation was performed for each sample with Illumina sequencing libraries containing 300–500 bp insert fragments, followed by sequencing on an Illumina NovaSeq 6000 platform at TsingKe Biotech Co., Ltd (Chengdu, China). The raw reads were quality-trimmed using fastp v.0.23.2[81] and then assembled into mitochondrial genomes with MitoFinder v.1.4.1[82] under default parameters, using *Troglonectes furcocaudalis* (GenBank: NC_073138) as the reference. For selected species, mitochondrial gene fragments (*CO1*, *Cyt b*, *16S*, *ND4*, and *ND5*) and nuclear gene fragments (*EGR1*, *EGR2B*, *EGR3*, *IRBP2*, *RAG1*, *RH1*, and *MYH6*) were amplified. PCR amplification for all samples was performed under the following conditions: initial denaturation at 98 °C for 3 min; followed by 35 cycles of denaturation at 95 °C for 30 s, annealing at 50–55 °C for 40 s, and extension at 72 °C for 1 min; with a final extension at 72 °C for 10 min. The corresponding PCR primers and detailed annealing temperatures are provided in Supplementary Table 1. Purified PCR products were directly sequenced in both directions using an ABI Prism 3730 automated DNA sequencer (Tsingke Biotech Co., Ltd., Chengdu, China). Mitochondrial genomes and fragments, as well as nuclear gene sequences, available in GenBank were retrieved to expand the sequence data matrix (Supplementary Tables 2–8; Supplementary Data 2–4).

Estimation of divergence times

Sequence alignment was performed with PhyloSuite v.1.2.3[83] using MAFFT v.7.520[84] for each gene fragment, followed by manual adjustments by MEGA v.7.0[85]. To ensure robust phylogenetic reconstruction and divergence time estimation, we utilized three main types of sequence matrices, depending on the available data for each specific lineage comparison: 1) concatenated mitochondrial and nuclear genes (Supplementary Data 3 and 4; Supplementary Tables 4–6); 2) concatenated mitochondrial genes only (Supplementary Tables 2, 3, and 7); 3) mitochondrial *Cyt b* gene only (Supplementary Table 8). PartitionFinder v.2.1.1 was used to identify the best-fit evolutionary model[86] under the Bayesian information criterion, where each gene segment was defined as a partition. For each dataset, the divergence times were estimated in BEAST v.2.4.7[87] using the uncorrelated relaxed molecular clock, a Yule prior, and the best-fit model. For our BEAST analyses, we employed a strategy combining fossil calibrations and secondary calibrations to derive time-calibrated phylogenies[88] (see the Supplementary Note 1 for more details). Tracer v.1.7.1[89] was used to assess an appropriate burn-in fraction and a sufficient effective sample size (> 200).

Biogeographic and habitat analyses

In southern China, the upper reaches of the Yangtze and Pearl Rivers demonstrate the highest species richness of cavefishes. We used the R package BioGeoBEARS[90] to infer the biotic interchange of cavefishes between these two river drainages based on dispersal–extinction–cladogenesis (DEC)[91], dispersal–vicariance analysis (DIVALIKE)[92], a Bayesian biogeographical inference model (BAYAREALIKE)[93], and the corresponding long-distance jumping (j) models. The six models were assessed using the time tree as the input (Supplementary Tables 9–11), and the optimal models were those with the maximum values of the log-likelihood and AICc model weights. A total of three major biogeographic regions were defined for ancestral region reconstruction: (1) the Pearl River basin, including the Beipanjiang, Guijiang–Hejiang, Hongshui, Jinshajiang, Liujiang, Nanpanjiang, Panlongjiang, and Zuojiang-Youjiang Rivers; (2) the Yangtze River basin, including the Wujiang and Yuanjiang Rivers, and (3) the rest of the world. The maximum range size was set to two.

The ancestral states of sister clade nodes were assessed using Bayesian Binary MCMC within RASP v.4.0[94] to infer the evolutionary origin of cavefishes following Li *et al.*[12]. The habitat status of each species was coded as cave-dwelling or epigean according to established criteria[22,23], based on actual surveys and reports in the literature (Supplementary Data 1). To minimize the effects of phylogenetic uncertainty, we used 2,000 trees obtained from the BEAST analyses and ran 1,000 sampling posterior distributions using a fixed JC + G model, with 10 simultaneous chains running for 5×10^6 generations[12].

Dynamic meta-analysis of lineage divergence

The dates of cave entry and the diversification dynamics of cavefishes were inferred using previously employed criteria [19,77] concerning the phylogeny to categorize events into four categories, i.e., migration into caves, dispersal, *in situ* diversification, and lineage divergence. The results of the BEAST and BBM analyses were then summarized to obtain the time intervals for the 95% confidence intervals (CIs) of these events. The respective events were defined as the maximum number of observed migrations into caves per 0.3 million years (MCE), the maximum number of observed dispersal events per 0.3 million years (MDisE), the maximum number of observed *in situ* diversification events per 0.3 million years (MDivE), and the maximum number of observed lineage divergence events per 0.3 million years (MDE)[18,19,77]. In addition, the exchange of taxa between the Pearl and Yangtze Rivers was divided into two types, i.e., Pearl River dispersal to the Yangtze River and vice versa.

To estimate the 95% confidence intervals for the origins, peaks, and valleys of the diversification curves, we generated 1,000 bootstrap pseudo-replicates from the original confidence intervals using the R package sample function. We then repeated the calculations to identify the origins and peaks of the MCE, MDE, MDivE, and MDisE curves. Diversification breakpoint detection was conducted in R v.4.2.2 using piecewise regression analysis[95] via the *segmented* package[96], with models containing one to three inflection points evaluated across 1000 bootstrap iterations based on the Bayesian Information Criterion (Supplementary Fig. 24, Supplementary Tables 12, 13, and 18). The model with the lowest Bayesian Information Criterion value[77] was selected. Once the optimal model was determined, 95% confidence intervals were calculated for each key inflection point.

Statistics and reproducibility

All statistical analyses were performed using R v.4.2.2. The event counts were obtained from biogeographic and ancestral trait reconstructions based on ten time-calibrated trees, using 95% confidence intervals of node divergence times, as detailed in the Methods. Diversification events were quantified by counting concurrent events at 0.3 Ma intervals over 45 Ma. Temporal patterns were smoothed using a 1.5 Ma moving average window. Descriptive statistics for each diversification event were calculated as the mean with its 95% confidence interval. Breakpoints in diversification rates were detected using piecewise regression, with model selection based on the Bayesian Information Criterion and confidence intervals estimated via bootstrap resampling (1,000 iterations). Statistical significance is indicated as follows: $p < 0.05$ (*), $p < 0.01$ (**), $p < 0.001$ (***), and $p < 0.0001$ (****). All tests were two-sided, with $p < 0.05$ considered statistically significant. The analyzed event types include dispersal (n = 49), *in situ* diversification (n = 307), migration into caves (n = 20), and lineage divergences (n = 190). For *in situ* diversification within river basins, the events are distributed as follows: Beipanjiang (n = 7), Guijiang-Hejiang (n = 10), Hongshui (n = 61), Jinshajiang (n = 11), Liujiang (n = 59), Nanpanjiang (n = 86), Panlongjiang (n = 5), Upper Yangtze-Wujiang (n = 19), Yuanjiang (n = 5), and Zuojiang-Youjiang (n = 22). Additionally, dispersal events from the Pearl River to the Yangtze River and the reverse dispersal number 7 and 6, respectively. Detailed information is provided in Supplementary Data 5 and 6. Analysis code is available in the Science Data Bank[88].

Data availability

The sequences reported in this paper have been deposited in GenBank (accession nos. ON116493–ON116532, ON148332–ON148334, OP473612–OP473909, OQ754141–OQ754145, OQ754148–OQ754150, OQ754152, OQ754154, OQ754155, OQ754157–OQ754159, PQ222367–PQ222376, PX715913–PX715924). All publicly available sequence data (e.g., GenBank accessions) used in this study are detailed in Supplementary Tables 1–8 and Supplementary Data 2–4. Source data underlying Fig. 1 are provided in Supplementary Data 1. Source data for Fig. 2 have been deposited in the Science Data Bank (https://doi.org/10.57760/sciencedb.35098)[88]. Source data for Fig. 3A, 3B, 3C, 3D, 3E, and 3F are provided in Supplementary Data 5, Supplementary Data 6, Supplementary Table 14, Supplementary Table 15, Supplementary Table 16, and PANGAEA (https://doi.org/10.1594/PANGAEA.917503)[39,97] (Supplementary Table 17), respectively. Source data underlying Fig. 4 are available in PANGAEA (https://doi.org/10.1594/PANGAEA.917503)[39,97] and included in Supplementary Table 17. All other datasets are provided in the supplementary information and data files associated with this publication. Source data for sequence alignments, time-calibrated phylogenies, diversification analyses, and paleoenvironmental reconstructions are available from the Science Data Bank. (https://doi.org/10.57760/sciencedb.35098).

Code availability

All analyses were conducted using open-source software tools, with detailed parameters specified in the corresponding methods sections Scripts used for generating the associated figures have been archived at Science Data Bank (https://doi.org/10.57760/sciencedb.35098).

References

1. Lu, H. *et al.* Formation and evolution of the Asian landscape during the Cenozoic. *Innov. Geosci.* **1**, 100020 (2023).
2. Ding, L. *et al.* Timing and mechanisms of Tibetan Plateau uplift. *Nat. Rev. Earth Environ.* **3**, 652–667 (2022).
3. Yuan, J. *et al.* Rapid drift of the Tethyan Himalaya terrane before two-stage India-Asia collision. *Natl. Sci. Rev.* **8**, nwaa173 (2021).
4. Luo, Y. & Li, S. The stepwise Indian–Eurasian collision and uplift of the Himalayan-Tibetan plateau drove the diversification of high-elevation Scytodes spiders. *Cladistics* **38**, 582–594 (2022).
5. Favre, A. *et al.* The role of the uplift of the Qinghai-Tibetan Plateau for the evolution of Tibetan biotas. *Biol. Rev.* **90**, 236–253 (2015).
6. Wu, F. *et al.* Reorganization of Asian climate in relation to Tibetan Plateau uplift. *Nat. Rev. Earth Environ.* **3**, 684–700 (2022).
7. Zheng, H. *et al.* Pre-Miocene birth of the Yangtze River. *Proc. Natl. Acad. Sci. U.S.A.* **110**, 7556–7561 (2013).
8. Zhang, Z. *et al.* Late Oligocene formation of the Pearl River triggered by the opening of the South China Sea. *Geophys. Res. Lett.* **50**, e2023GL103049 (2023).
9. Spicer, R. A. Tibet, the Himalaya, Asian monsoons and biodiversity–In what ways are they related? *Plant Divers.* **39**, 233–244 (2017).
10. Ding, W. N., Ree, R. H., Spicer, R. A. & Xing, Y. W. Ancient orogenic and monsoon-driven assembly of the world's richest temperate alpine flora. *Science* **369**, 578–581 (2020).
11. Che, Y. & Yu, J. *Karst in China*. 81–95 (Science Press, 1985).
12. Li, X. Q. *et al.* Biotic colonization of subtropical East Asian caves through time. *Proc. Natl. Acad. Sci. U.S.A.* **119**, e2207199119 (2022).
13. Wen, H. *et al.* Molecular phylogeny and historical biogeography of the cave fish genus *Sinocyclocheilus* (Cypriniformes: Cyprinidae) in southwest China. *Integr. Zool.* **17**, 311–325 (2022).
14. Stokes, M. F. *et al.* Erosion of heterogeneous rock drives diversification of Appalachian fishes. *Science* **380**, 855–859 (2023).
15. Hoorn, C., Mosbrugger, V., Mulch, A. & Antonelli, A. Biodiversity from mountain building. *Nat. Geosci.* **6**, 154–154 (2013).
16. Rahbek, C. *et al.* Humboldt's enigma: What causes global patterns of mountain biodiversity? *Science* **365**, 1108–1113 (2019).
17. Rahbek, C. *et al.* Building mountain biodiversity: geological and evolutionary processes. *Science* **365**, 1114–1119 (2019).
18. Klaus, S., Morley, R. J., Plath, M., Zhang, Y.-P. & Li, J.-T. Biotic interchange between the Indian subcontinent and mainland Asia through time. *Nat. Commun.* **7**, 12132 (2016).
19. Xu, W. *et al.* Herpetological phylogeographic analyses support a Miocene focal point of Himalayan uplift and biological diversification. *Natl. Sci. Rev.* **8**, nwaa263 (2021).
20. White, W. B. & Culver, D. C. in *Encyclopedia of Caves (Third Edition)*. *Cave, Definition of* (eds William B. White, David C. Culver, & Tanja Pipan) Ch. 29, 255–259 (Academic Press, 2019).
21. Borowsky, R. Cavefishes. *Curr. Biol.* **28**, R60–R64 (2018).
22. Zhao, Y. H., Gozlan, R. E. & Zhang, C. G. Out of sight out of mind: current knowledge of Chinese cave fishes. *J. Fish Biol.* **79**, 1545–1562 (2011).
23. Ma, L., Zhao, Y. H. & Yang, J. X. in *Encyclopedia of Caves (Third Edition)*. *Cavefish of China* (eds William B. White, David C. Culver, & Tanja Pipan) Ch. 28, 237–254 (Academic Press, 2019).
24. Mao, T. R. *et al.* Evolution in *Sinocyclocheilus* cavefish is marked by rate shifts, reversals, and origin of novel traits. *BMC Ecol. Evol.* **21**, 1–14 (2021).
25. Mao, T. *et al.* Evolving in the darkness: phylogenomics of *Sinocyclocheilus* cavefishes highlights recent diversification and cryptic diversity. *Mol. Phylogenet. Evol.* **168**, 107400 (2022).
26. Shu, S. S., Jiang, W. S., Whitten, T., Yang, J. X. & Chen, X. Y. Drought and China's cave species. *Science* **340**, 272–

272 (2013).

27. Duan, Y. F., Li, M., Xu, K. W., Zhang, L. & Zhang, L. B. Protect China's karst cave habitats. *Science* **374**, 699–699 (2021).
28. Wu, L. *et al.* A long-ignored unique ecosystem of cavefishes in the southern karst: Achievements, challenges, and prospects. *Environ. Sci. Pollut. Res.* **30**, 90489–90499 (2023).
29. Mao, T. *et al.* Caves as Species Pumps: Key Innovations, Isolation and Periodic Introgression Drive the World's Largest Cavefish Radiation in a Dynamic Karstic Landscape. *Mol. Ecol.* **34**, e70038 (2025).
30. Lee, T. Y. & Lawver, L. A. Cenozoic plate reconstruction of Southeast Asia. *Tectonophysics* **251**, 85–138 (1995).
31. Chung, S. L. *et al.* Tibetan tectonic evolution inferred from spatial and temporal variations in post-collisional magmatism. *Earth Sci. Rev.* **68**, 173–196 (2005).
32. Leloup, P. H. *et al.* New constraints on the structure, thermochronology, and timing of the Ailao Shan-Red River shear zone, SE Asia. *J. Geophys. Res.: Solid Earth* **106**, 6683–6732 (2001).
33. Schärer, U., Lian-Sheng, Z. & Tapponnier, P. Duration of strike-slip movements in large shear zones: The Red River belt, China. *Earth Planet. Sci. Lett.* **126**, 379–397 (1994).
34. Li, S. *et al.* Oligocene Deformation of the Chuandian Terrane in the SE Margin of the Tibetan Plateau Related to the Extrusion of Indochina. *Tectonics* **39**, e2019TC005974 (2020).
35. Li, X. Q. *et al.* Phylogenetic evidence clarifies the history of the extrusion of Indochina. *Proc. Natl. Acad. Sci. U.S.A.* **121**, e2322527121 (2024).
36. Liu, X., Hou, J. & You, X. Neotectonic motion of Youjiang fault zone. *J. Seismol. Res.* **10**, 175–183 (1987).
37. Nie, G., Yang, S., Zhang, P. & Li, B. Characteristics and Tectonic Significance of Cenozoic Strike-slip Faults in Youjiang Region. *Geotecton. Metallog.* **43**, 1094–1105 (2019).
38. Judd, E. J. *et al.* A 485-million-year history of Earth's surface temperature. *Science* **385**, eadk3705 (2024).
39. Westerhold, T. *et al.* An astronomically dated record of Earth's climate and its predictability over the last 66 million years. *Science* **369**, 1383–1387 (2020).
40. Luo, T. *et al.* Rapid speciation of Chinese hypogean fishes driven by paleogeoclimatic and morphological adaptations. *Curr. Zool.* **71**, 715–732 (2025).
41. Ma, Z. *et al.* Head Horn Enhances Hydrodynamic Perception in Eyeless Cavefish. *Adv. Sci.* **11**, 2406707 (2024).
42. Zhang, M. *et al.* A Splicing Mutation in mitfa is Involved in the Depigmentation of Cavefish *Triplophysa rosa*. *Mol. Biol. Evol.* **42**, msaf175 (2025).
43. Lam, S. M. *et al.* Quantitative Lipidomics and Spatial MS-Imaging Uncovered Neurological and Systemic Lipid Metabolic Pathways Underlying Troglomorphic Adaptations in Cave-Dwelling Fish. *Mol. Biol. Evol.* **39**, msac050 (2022).
44. Ding, W. *et al.* Palaeovegetation variation in response to the late Oligocene-early Miocene East Asian summer monsoon in the Ying-Qiong Basin, South China Sea. *Palaeogeogr. Palaeoclimatol. Palaeoecol.* **567**, 110205 (2021).
45. Ren, J., Schubert, B. A., Lukens, W. E. & Quan, C. Low oxygen isotope values of fossil cellulose indicate an intense monsoon in East Asia during the late Oligocene. *Palaeogeogr. Palaeoclimatol. Palaeoecol.* **577**, 110556 (2021).
46. Vornlocher, J. R., Lukens, W. E., Schubert, B. A. & Quan, C. Late Oligocene precipitation seasonality in East Asia based on $\delta^{13}C$ profiles in fossil wood. *Paleoceanogr. Paleoclimatol.* **36**, e2021PA004229 (2021).
47. Chen, C. *et al.* Lower-altitude of the Himalayas before the mid-Pliocene as constrained by hydrological and thermal conditions. *Earth Planet. Sci. Lett.* **545**, 116422 (2020).
48. Leloup, P. H. *et al.* The Ailao Shan-Red river shear zone (Yunnan, China), tertiary transform boundary of Indochina. *Tectonophysics* **251**, 3–84 (1995).
49. Tapponnier, P. *et al.* The Ailao Shan/Red River metamorphic belt: tertiary left-lateral shear between Indochina and South China. *Nature* **343**, 431–437 (1990).
50. Farnsworth, A. *et al.* Past East Asian monsoon evolution controlled by paleogeography, not CO_2. *Sci. Adv.* **5**, eaax1697 (2019).
51. Zhang, Q. *et al.* East Asian winter monsoon intensification over the Northwest Pacific Ocean driven by late Miocene

atmospheric CO_2 decline. *Sci. Adv.* **10**, eadm8270 (2024).

52. Wan, S. *et al.* Interactive forces of temperature and topographic uplift shaped the East Asian monsoon rainfall evolution since the Oligocene. *Innov. Geosci.* **3**, 100141 (2025).
53. Wang, Y. *et al.* Cenozoic exhumation of the Ailaoshan-Red River shear zone: New insights from low-temperature thermochronology. *Tectonics* **39**, e2020TC006151 (2020).
54. Zhang, J., Zhong, D., Sang, H. & Zhou, Y. Structural and Geochronological Evidence for Multiple Episodes of Tertiary Deformation along the Ailaoshan-Red River Shear Zone, Southeastern Asia, Since the Paleocene. *Acta Geol. Sin. Engl. Ed.* **80**, 79–96 (2006).
55. Jolivet, M. & Boulvais, P. Global significance of oxygen and carbon isotope compositions of pedogenic carbonates since the Cretaceous. *Geosci. Front.* **12**, 101132 (2021).
56. Liu, Y. *et al.* New chronological constraints on the Plio-Pleistocene uplift of the Guizhou Plateau, SE margin of the Tibetan Plateau. *Quat. Geochronol.* **67**, 101237 (2022).
57. Luo, T. *et al.* Phylogenetic relationships of Nemacheilidae cavefish (*Heminoemacheilus*, *Oreonectes*, *Yunnanilus*, *Paranemachilus*, and *Troglonectes*) revealed by analysis of mitochondrial genome and seven nuclear genes. *Zool. Res.* **44**, 693−697 (2023).
58. Ding, L. *et al.* Quantifying the rise of the Himalaya orogen and implications for the South Asian monsoon. *Geology* **45**, 215–218 (2017).
59. Zhang, B. *et al.* Comparative genomics reveals the hybrid origin of a macaque group. *Sci. Adv.* **9**, eadd3580 (2023).
60. Jensen, A. *et al.* Complex Evolutionary History With Extensive Ancestral Gene Flow in an African Primate Radiation. *Mol. Biol. Evol.* **40**, msad247 (2023).
61. Wang, X. *et al.* Phylogenomics reveals the evolution, biogeography, and diversification history of voles in the Hengduan Mountains. *Commun. Biol.* **5**, 1124 (2022).
62. Foley, N. M. *et al.* Karyotypic stasis and swarming influenced the evolution of viral tolerance in a species-rich bat radiation. *Cell Genomics* **4**, 100482 (2024).
63. Qian, Y. *et al.* The role of introgression during the radiation of endemic fishes adapted to living at extreme altitudes in the Tibetan Plateau. *Mol. Biol. Evol.* **40**, msad129 (2023).
64. Svardal, H. *et al.* Ancestral Hybridization Facilitated Species Diversification in the Lake Malawi Cichlid Fish Adaptive Radiation. *Mol. Biol. Evol.* **37**, 1100–1113 (2020).
65. He, J. *et al.* Evolution of eastern Asia river systems reconstructed by the mineralogy and detrital-zircon geochronology of modern Red River and coastal Vietnam river sand. *Earth Sci. Rev.* **245**, 104572 (2023).
66. Gilley, L. D. *et al.* Direct dating of left-lateral deformation along the Red River shear zone, China and Vietnam. *J. Geophys. Res.: Solid Earth* **108**, 2127 (2003).
67. Fyhn, M. B. & Phach, P. V. Late Neogene structural inversion around the northern Gulf of Tonkin, Vietnam: Effects from right-lateral displacement across the Red River fault zone. *Tectonics* **34**, 290–312 (2015).
68. Zhang, B., Liu, R., Xiang, H., Wan, J. & Huang, X. FT dating of fault rocks in the central-southern section of the Red River Fault zone and its geological implications. *Seismol. Geol.* **31**, 44–56 (2009).
69. Clift, P. D. *et al.* Correlation of Himalayan exhumation rates and Asian monsoon intensity. *Nat. Geosci.* **1**, 875–880 (2008).
70. Replumaz, A., Lacassin, R., Tapponnier, P. & Leloup, P. Large river offsets and Plio-Quaternary dextral slip rate on the Red River fault (Yunnan, China). *J. Geophys. Res.: Solid Earth* **106**, 819–836 (2001).
71. Fu, X. *et al.* The present-day Yangtze River was established in the late Miocene: Evidence from detrital zircon ages. *J. Asian Earth Sci.* **205**, 104600 (2021).
72. Zheng, H. *et al.* Formation of the First Bend in the late Eocene gave birth to the modern Yangtze River, China. *Geology* **49**, 35–39 (2021).
73. Chen, F. *et al.* Evolution of the Yangtze River and its biodiversity. *Innovation* **4**, 100417 (2023).
74. Clift, P. D. *et al.* A Late Eocene-Oligocene Through-Flowing River Between the Upper Yangtze and South China Sea. *Geochem. Geophys. Geosyst.* **21**, e2020GC009046 (2020).

75. Zhou, Q. & Chen, P. Lithofacies change and palaeogeographical evolution during Late Cenozoic in Guizhou and its vicinity. *Geol. Guizhou* **10**, 201–207 (1993).
76. Luo, T. *et al.* Evolutionary history of Chinese karst loaches (Nemacheilidae, *Karstsinnectes*): new insights from mitochondrial-based genomes and description of a new species from Guangxi, China. *Zoosyst. Evol.* **100**, 1473–1486 (2024).
77. Zhang, J. *et al.* Evolutionary history of the Arctic flora. *Nat. Commun.* **14**, 4021 (2023).
78. Lu, C. *et al.* Contrasting evolutionary trajectories of terrestrial vertebrates in the Hengduan Mountains hotspot. *Natl. Sci. Rev.* **12**, nwaf157 (2025).
79. Cao, G. L. *et al.* Cenozoic geoclimatic changes drove the evolutionary dynamics of floristic endemism on the Qinghai–Tibet Plateau. *Proc. Natl. Acad. Sci. U.S.A.* **122**, e2426017122 (2025).
80. Jiang, D., Klaus, S., Zhang, Y.-P., Hillis, D. M. & Li, J.-T. Asymmetric biotic interchange across the Bering land bridge between Eurasia and North America. *Natl. Sci. Rev.* **6**, 739-745 (2019).
81. Chen, S., Zhou, Y., Chen, Y. & Gu, J. fastp: an ultra-fast all-in-one FASTQ preprocessor. *Bioinformatics* **34**, i884–i890 (2018).
82. Allio, R. *et al.* MitoFinder: Efficient automated large-scale extraction of mitogenomic data in target enrichment phylogenomics. *Mol. Ecol. Resour.* **20**, 892–905 (2020).
83. Zhang, D. *et al.* PhyloSuite: An integrated and scalable desktop platform for streamlined molecular sequence data management and evolutionary phylogenetics studies. *Mol. Ecol. Resour.* **20**, 348–355 (2020).
84. Katoh, K. & Standley, D. M. MAFFT multiple sequence alignment software version 7: improvements in performance and usability. *Mol. Biol. Evol.* **30**, 772–780 (2013).
85. Kumar, S., Stecher, G. & Tamura, K. MEGA7: molecular evolutionary genetics analysis version 7.0 for bigger datasets. *Mol. Biol. Evol.* **33**, 1870–1874 (2016).
86. Lanfear, R., Frandsen, P. B., Wright, A. M., Senfeld, T. & Calcott, B. PartitionFinder 2: new methods for selecting partitioned models of evolution for molecular and morphological phylogenetic analyses. *Mol. Biol. Evol.* **34**, 772–773 (2017).
87. Bouckaert, R. *et al.* BEAST 2: a software platform for Bayesian evolutionary analysis. *PLoS Comput. Biol.* **10**, e1003537 (2014).
88. Luo, T. *et al. Evolutionary history of Chinese cavefishes parallels paleogeoclimatic and river capture processes* [Data set]. Science Data Bank https://doi.org/10.57760/sciencedb.35098 (2026).
89. Rambaut, A., Drummond, A. J., Xie, D., Baele, G. & Suchard, M. A. Posterior summarization in Bayesian phylogenetics using Tracer 1.7. *Syst. Biol.* **67**, 901–904 (2018).
90. Matzke, N. J. Probabilistic historical biogeography: new models for founder-event speciation, imperfect detection, and fossils allow improved accuracy and model-testing. *Front. Biogeogr.* **5**, 242–248 (2013).
91. Ree, R. H. & Smith, S. A. Maximum likelihood inference of geographic range evolution by dispersal, local extinction, and cladogenesis. *Syst. Biol.* **57**, 4−14 (2008).
92. Ronquist, F. Dispersal-vicariance analysis: a new approach to the quantification of historical biogeography. *Syst. Biol.* **46**, 195–203 (1997).
93. Landis, M. J., Matzke, N. J., Moore, B. R. & Huelsenbeck, J. P. Bayesian analysis of biogeography when the number of areas is large. *Syst. Biol.* **62**, 789–804 (2013).
94. Yu, Y., Blair, C. & He, X. RASP 4: ancestral state reconstruction tool for multiple genes and characters. *Mol. Biol. Evol.* **37**, 604–606 (2020).
95. Muggeo, V. M. Estimating regression models with unknown break-points. *Stat. Med.* **22**, 3055–3071 (2003).
96. Muggeo, V. M. Segmented: an R package to fit regression models with broken-line relationships. *R News* **8**, 20–25 (2008).
97. Westerhold, T. *Cenozoic global reference benthic carbon and oxygen isotope dataset (CENOGRID)* [Data set]. PANGAEA https://doi.org/10.1594/PANGAEA.917503 (2020).
98. Jiang, Z. C. *et al.* Calculation of atmospheric CO_2 sink formed in karst progresses of the karst divided regions in China.

Carsolog. Sin. **30**, 363–367 (2011).

99. Clift, P. D. Controls on the erosion of Cenozoic Asia and the flux of clastic sediment to the ocean. *Earth Planet. Sci. Lett.* **241**, 571–580 (2006).

Acknowledgements

This work was supported by the following programs: the Endangerment Processes and Mechanisms of Endangered Flagship Animals (2022YFF1301502), the Strategic Priority Research Program of the Chinese Academy of Sciences (CAS) (XDB31000000), and the Guizhou Normal University Academic Emerging Talent Fund Project (Qianshi Xin Miao [2021] 20). We are grateful to Prof. Li-Na Du for providing tissue samples of *Karstsinnectes longzhouensis* and *Troglonectes hechiensis*. We are grateful to Mr. Jia-Hu Lan for providing tissue samples of *Karstsinnectes acridorsalis* and *Troglonectes barbatus* used in this study. We also thank Chang-Ting Lan, Jing Yu, Ya-Li Wang, Xin-Rui Zhao, Xing-Liang Wang, Zhi-Xia Chen, and Ming-Le Mao for their assistance in field surveys and laboratory work. We thank LetPub (www.letpub.com.cn) for its linguistic assistance during the preparation of this manuscript.

Author Contributions

T.L.: data curation, formal analysis, investigation, methodology, visualization, writing—original draft, writing—review and editing; M.Y.X.: conceptualization, data curation, investigation, methodology, project administration, supervision, visualization, writing—review and editing; M.L. and J. J.W.: data curation; N.X.: writing—review and editing; J.Z.: conceptualization, formal analysis, funding acquisition, investigation, methodology, project administration, resources, supervision, visualization, writing—review and editing. All authors gave final approval for publication and agreed to be held accountable for the work performed therein.

Ethics Statement

All authors have approved the manuscript content, author list and order, and contribution statements. Sample collection complied with China's wildlife protection laws and regulations. The sampling procedures followed the National Standards of the People's Republic of China (GB/T 39760-2021; GB/T 35892-2018) and the Guidelines for the Care and Use of Laboratory Animals established by the Ethics Committee of Guizhou Normal University (Guiyang, Guizhou, China).

Competing interests

The authors declare no competing interests.

Additional information

Supplementary information

The online version contains supplementary material available in this manuscript.

Figure and Table captions

Fig. 1 Map of study area. **(A)** Spatial patterns of species diversity of cavefishes as measured by the number of species. The purple line denotes the Ailao Shan–Red River shear zone (ARSZ). The inset images show representative cavefish from southwestern China: *Sinocyclocheilus microphthalmus* (top) and *Troglonectes microphthalmus* (bottom, photo by Mr. Jia-Hu Lan). The karst distribution was referenced from Jiang et al[98]. **(B)** Hydrology of the upper Yangtze and Pearl Rivers. Abbreviation: GHR, Guijiang-Hejiang River; LJR, Liujiang River; HSR, Hongshui River; ZYR, Zuojiang-Youjiang River, BPR, Beipanjiang River, NPR, Nanpanjiang River; UYR, upper Yangtze River; YJR, Yuanjiang River; WJR, Wujiang River; CSR, Chishui River; JSR, Jinshajiang River; DMR, Dadu-Minjiang River; PLR, Panlongjiang River; LXR, Lixianjiang River; YR, Yuan River. **(C)** Map of the Youjiang region showing the distribution of fault zones[37].

Fig. 2 An overview of the time tree used for the phylogeographic analysis. The red color indicates cave species.

Fig. 3 Dynamic rates of Chinese cavefish diversification and the potential driving factors. **(A)** The rates of dispersal (n=49 events), *in situ* diversification (n=307 events), migration into caves (n=20 events), and lineage divergences (n=190 events) through time. The S1–S3 phases were modified from the three-phase hypothesis of karst evolution in southern China proposed by Che and Yu[11]. The grey rectangular boxes represent time frames that are not included in the three phases. **(B)** *In situ* diversification dynamics in different drainages, based on the maximum number of observed *in situ* diversification events per million years (MDivE). Beipanjiang (n= seven events), Guijiang-Hejiang (n= ten events), Hongshui (n= 61 events), Jinshajiang (n= 11 events), Liujiang (n= 59 events), Nanpanjiang (n= 86 events), Panlongjiang (n= five events), Upper Yangtze-Wujiang (n= 19 events), Yuanjiang (n= four events), Zuojiang-Youjiang (n= 22 events). **(C)** Dispersal dynamics based on the observed maximum number of dispersal events per Ma (MDisE) between the Yangtze and Pearl River basins. Pearl to Yangtze (n= seven events) and Yangtze to Pearl (n= six events). Erosion data modified from Wan et al.[52] **(D)** The stepwise uplift history of the Qinghai–Tibet Plateau (QTP), showing the Himalayas and the India–Asia suture, the Lhasa–Qiangtang suture valley, and the eastern QTP[2]. Error bars indicate the range of temporal and corresponding paleoelevation data. **(E)** Evolutionary dynamics of the sediment budget in the Pearl River/South China basins[99]. **(F)** Illustration of climatic evolution from the late Eocene to the present, showing global climate (deep-sea oxygen isotope records ($\delta^{18}O$) (dark grey)[39] and estimated ocean temperatures (orange)[50]) and East Asian monsoon conditions (mean annual precipitation at idealized CO_2 levels[39]). The cross-shaped symbols represent individual data points of the $\delta^{18}O$ values. **(G)** The uplift history and expected biotic assembly processes of the QTP since ~60 Ma, Refer to Ding et al.[58] and Xu et al.[19]. The red solid circles denote key time points. The Stepwise Hypothesis posits that the QTP initiated its uplift during the early Paleocene through a series of stepwise uplift events, with accelerated uplift occurring later during the Miocene (23–15 Ma) before reaching its present elevation. In contrast, the Late Orogeny Hypothesis proposes that the QTP began its major uplift in the early Miocene and reached the current elevations much later (~7.0–3.2 Ma). Abbreviation: Pli., Pliocene; Q., Quaternary.

Fig. 4 Evolution of karst cavefish in southwestern China in relation to climatic and geological history. **(A)** Major events associated with cavefish diversification and their relative contributions. **(B)** Adaptive evolution in morphology and genetics has shaped the diverse and unique cave biota in cavefishes. **(C)** Schematic representation of karst cave and cavefish formation across four evolutionary phases from the late Eocene to the present. Illustration of climatic evolution from the late Eocene to the present, showing global climate (deep-sea oxygen isotope records ($\delta^{18}O$) (dark grey)[39] and estimated ocean temperatures (orange)[50]) and East Asian monsoon conditions (mean annual precipitation at idealized CO_2 levels[39]). The data used to plot the paleoclimate are the same as in Figure 3F, but are only shown for 35 Ma to the present. The schematic uplift of the Qinghai–Tibet Plateau (QTP) illustrates how tectonic processes created extensive fragmented subterranean landscapes, providing ecological opportunities for *in situ* diversification of cavefish (reference to Ding et al.[2]). Light blue lines indicate rivers. The phylogenetic diagram indicates the relative number of *in situ* speciation events (reference to Lu et al.[78]). Abbreviation: Morph, Morphology; Genet, Genetics; De-evo, De-evolution; Co-evo, Co-evolution; Ada-evo, Adaptive-evolution; Pli., Pliocene; Q., Quaternary.

Table 1. Numbers and mean ages of cavefishes involved in various biogeographic events and their 95% confidence intervals.

Biogeographic event type	Number	Mean age (95% CI) (Ma)
Dispersal	49	10.0 (12.3–8.0)
In situ diversification	307	8.0 (8.9–7.2)
Migrations into caves	20	20.9 (27.8–14.7)
Migration outside the caves	190	8.2 (9.3–7.1)
Lineage divergences	2	19.9 (20.6–19.3)
From Pearl River dispersal to Yangtze River	7	11.3 (16.0–6.1)
From Yangtze River dispersal to Pearl River	6	6.2 (7.9–4.7)

Editorial Summary: An integrated multi-taxa biogeographic analysis of 183 cavefish species endemic to China suggest that the origin and diversification of cavefishes are closely linked to the evolution of karst landscape since the late Eocene.

Peer Review Information: *Communications Biology* thanks Xidong Mu and the other, anonymous, reviewer(s) for their contribution to the peer review of this work. Primary Handling Editor: George Inglis. [A peer review file is available.]

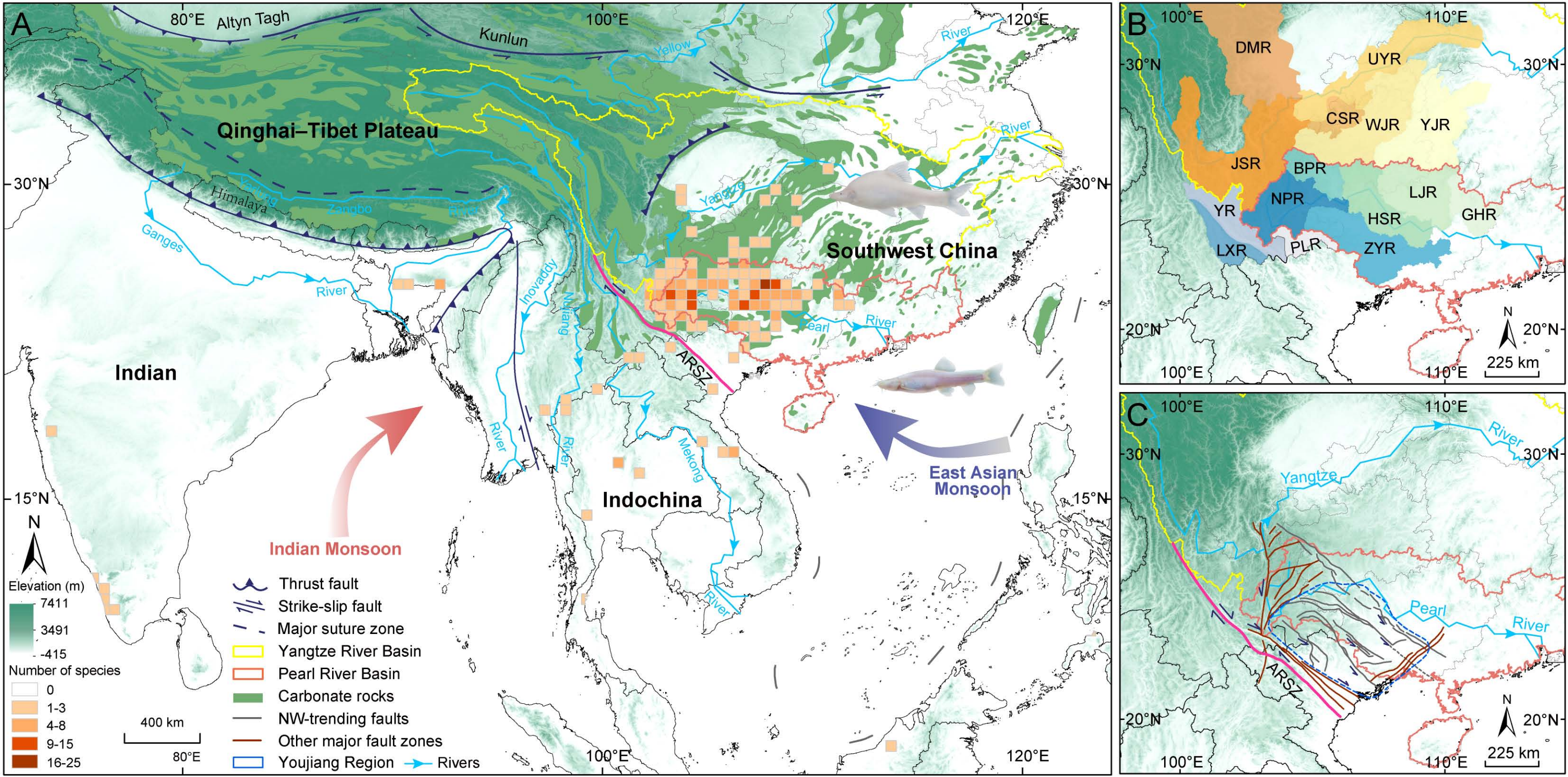
A
80°E
100°E
120°E
30°N
15°N
Altyn Tagh
Kunlun
Yellow
River
Qinghai–Tibet Plateau
Himalaya
Yarlung
Zangbo
River
Ganges
River
Yangtze
River
Inovaddy
Nujiang
River
Pearl
River
Mekong
River
ARSZ
Southwest China
Indian
Indochina
Indian Monsoon
East Asian Monsoon
N
400 km
Elevation (m)
7411
3491
-415
Number of species
0
1-3
4-8
9-15
16-25
Thrust fault
Strike-slip fault
Major suture zone
Yangtze River Basin
Pearl River Basin
Carbonate rocks
NW-trending faults
Other major fault zones
Youjiang Region
Rivers
B
100°E
110°E
30°N
20°N
DMR
UYR
CSR
WJR
YJR
JSR
BPR
NPR
LJR
YR
HSR
GHR
LXR
PLR
ZYR
N
225 km
C
100°E
110°E
30°N
20°N
Yangtze
River
Pearl
River
ARSZ
N
225 km

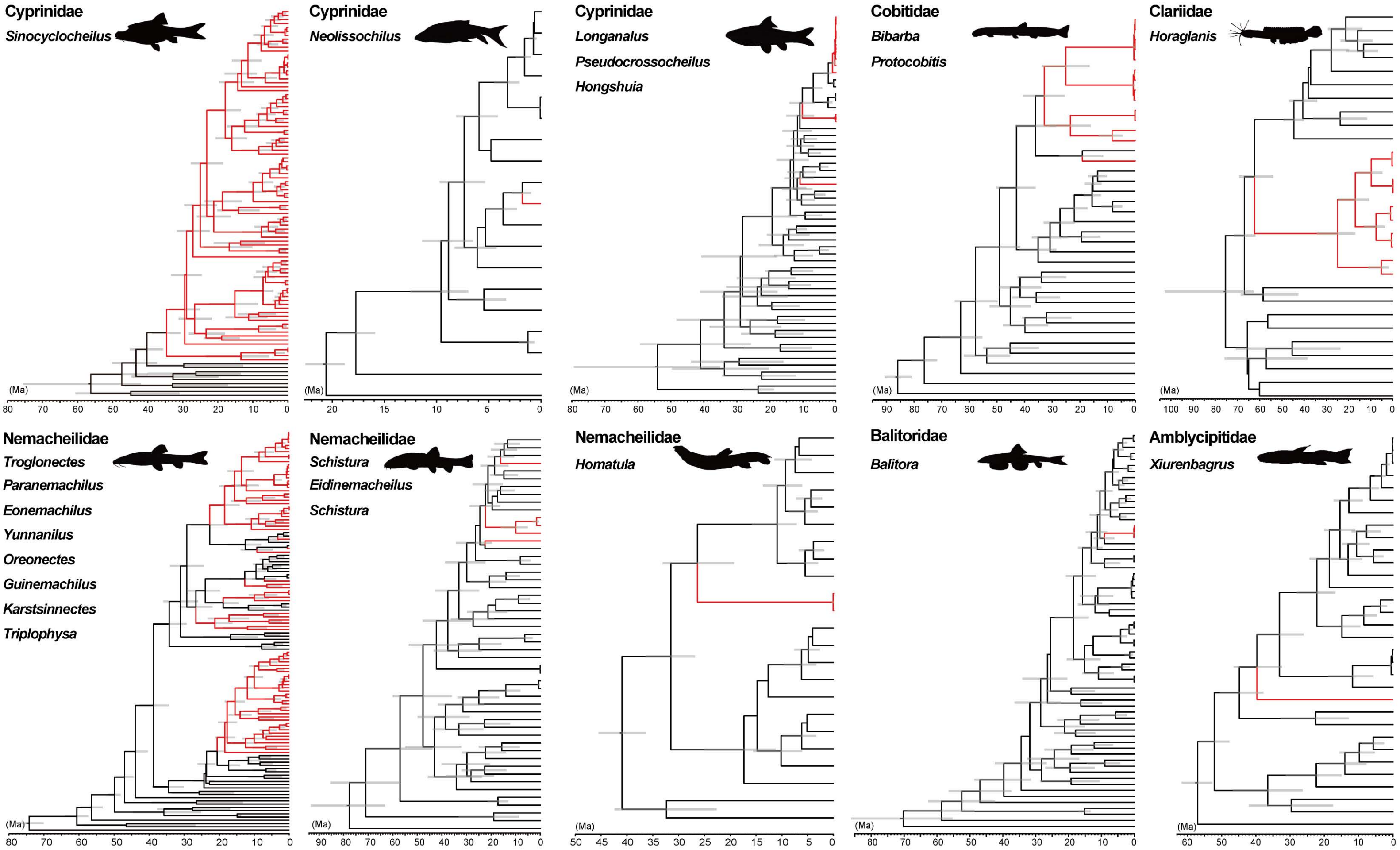
Cyprinidae
Sinocyclocheilus
(Ma)
80 70 60 50 40 30 20 10 0
Cyprinidae
Neolissochilus
(Ma)
20 15 10 5 0
Cyprinidae
Longanalus
Pseudocrossocheilus
Hongshuia
(Ma)
80 70 60 50 40 30 20 10 0
Cobitidae
Bibarba
Protocobitis
(Ma)
90 80 70 60 50 40 30 20 10 0
Clariidae
Horaglanis
(Ma)
100 90 80 70 60 50 40 30 20 10 0
Nemacheilidae
Troglonectes
Paranemachilus
Eonemachilus
Yunnanilus
Oreonectes
Guinemachilus
Karstsinnectes
Triplophysa
(Ma)
80 70 60 50 40 30 20 10 0
Nemacheilidae
Schistura
Eidinemacheilus
Schistura
(Ma)
90 80 70 60 50 40 30 20 10 0
Nemacheilidae
Homatula
(Ma)
50 45 40 35 30 25 20 15 10 5 0
Balitoridae
Balitora
(Ma)
80 70 60 50 40 30 20 10 0
Amblycipitidae
Xiurenbagrus
(Ma)
60 50 40 30 20 10 0

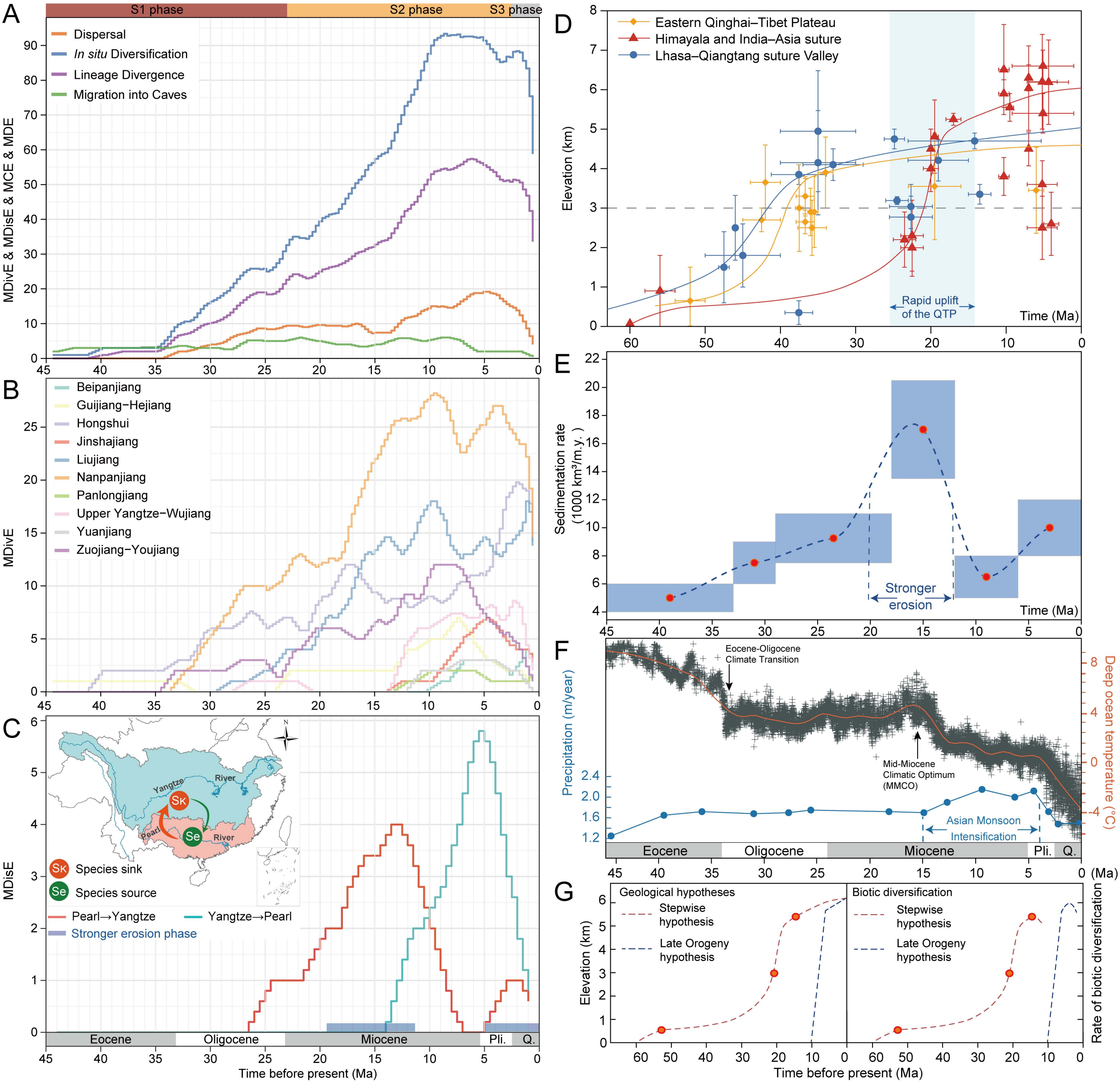
A
S1 phase
S2 phase
S3 phase
Dispersal
In situ Diversification
Lineage Divergence
Migration into Caves
MDivE & MDisE & MCE & MDE
B
Beipanjiang
Guijiang−Hejiang
Hongshui
Jinshajiang
Liujiang
Nanpanjiang
Panlongjiang
Upper Yangtze−Wujiang
Yuanjiang
Zuojiang−Youjiang
MDivE
C
Yangtze
River
Pearl
River
Sk
Se
Species sink
Species source
Pearl→Yangtze
Yangtze→Pearl
Stronger erosion phase
MDisE
Eocene
Oligocene
Miocene
Pli.
Q.
Time before present (Ma)
D
Eastern Qinghai–Tibet Plateau
Himayala and India–Asia suture
Lhasa–Qiangtang suture Valley
Elevation (km)
Rapid uplift of the QTP
Time (Ma)
E
Sedimentation rate (1000 km³/m.y.)
Stronger erosion
Time (Ma)
F
Eocene-Oligocene Climate Transition
Mid-Miocene Climatic Optimum (MMCO)
Asian Monsoon Intensification
Precipitation (m/year)
Deep ocean temperature (°C)
Eocene
Oligocene
Miocene
Pli.
Q.
(Ma)
G
Geological hypotheses
Stepwise hypothesis
Late Orogeny hypothesis
Biotic diversification
Stepwise hypothesis
Late Orogeny hypothesis
Elevation (km)
Rate of biotic diversification
Time before present (Ma)

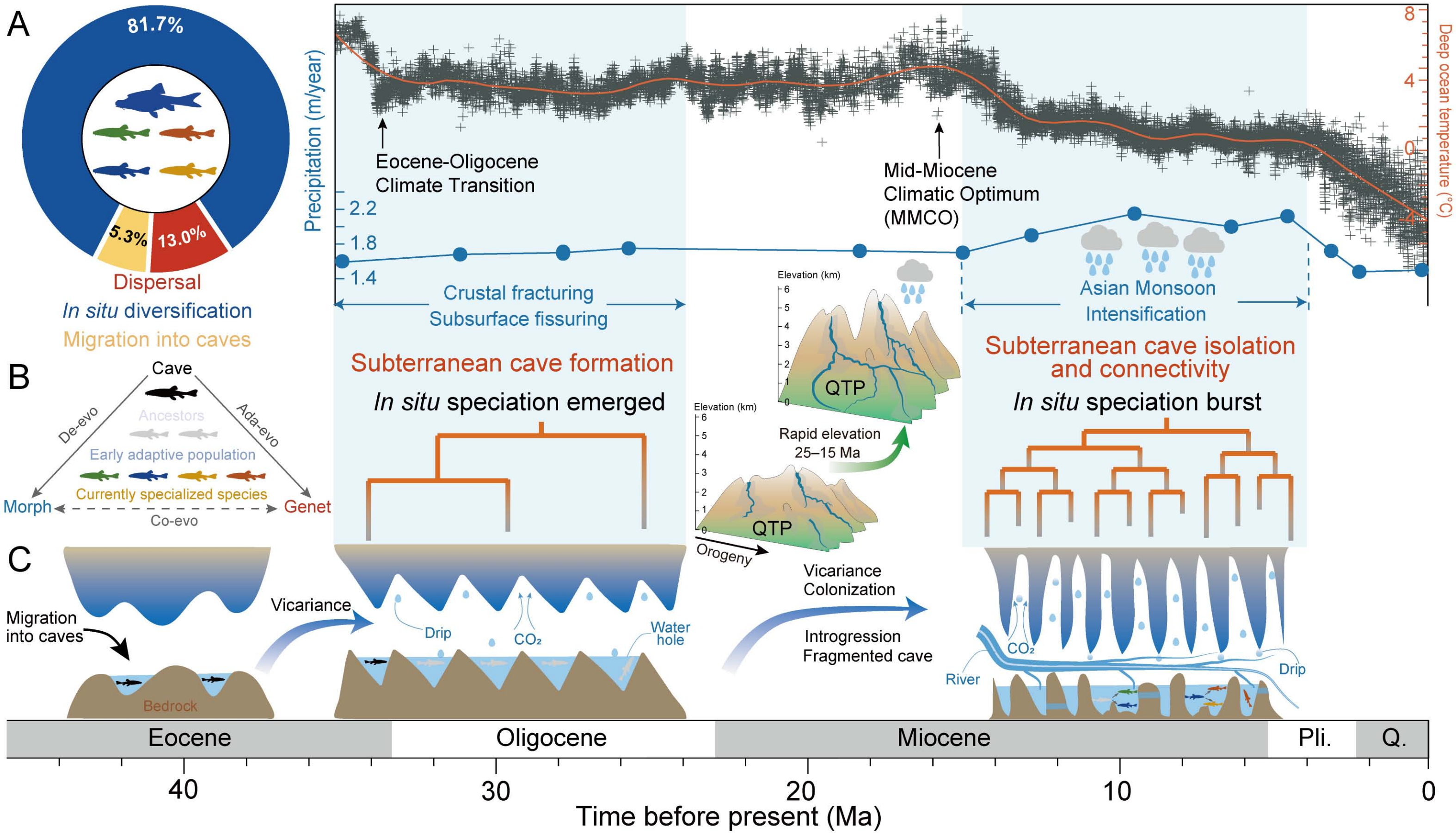
A
81.7%
5.3%
13.0%
Dispersal
In situ diversification
Migration into caves
Precipitation (m/year)
2.2
1.8
1.4
Deep ocean temperature (°C)
8
4
0
-4
Eocene-Oligocene
Climate Transition
Mid-Miocene
Climatic Optimum
(MMCO)
Crustal fracturing
Subsurface fissuring
Asian Monsoon
Intensification
Subterranean cave formation
In situ speciation emerged
Subterranean cave isolation
and connectivity
In situ speciation burst
Elevation (km)
6
5
4
3
2
1
0
QTP
Rapid elevation
25–15 Ma
Orogeny
B
Cave
De-evo
Ada-evo
Ancestors
Early adaptive population
Currently specialized species
Morph
Genet
Co-evo
C
Migration
into caves
Bedrock
Vicariance
Drip
CO₂
Water
hole
Vicariance
Colonization
Introgression
Fragmented cave
River
Drip
Eocene
Oligocene
Miocene
Pli.
Q.
40
30
20
10
0
Time before present (Ma)

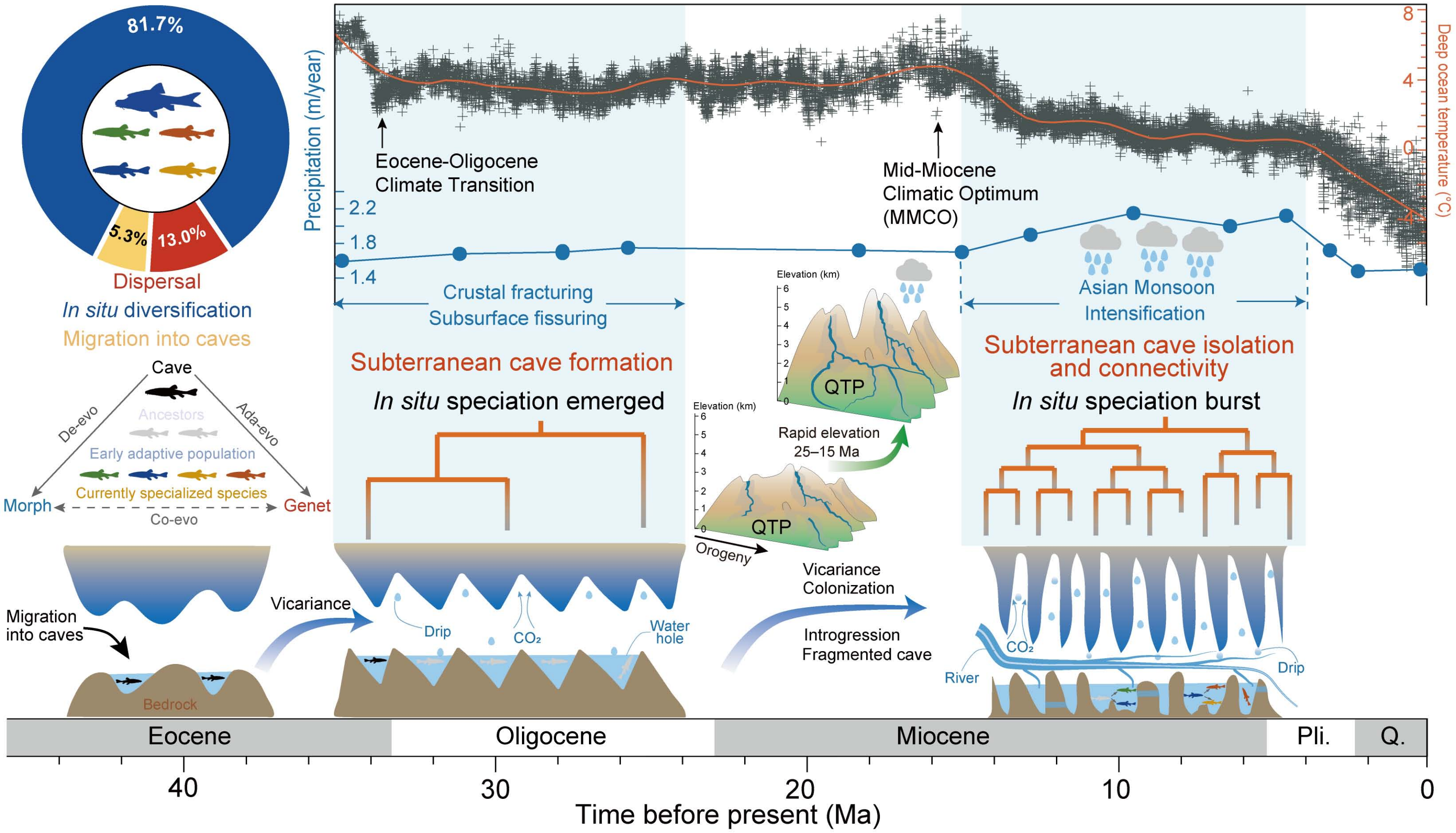
81.7%
5.3%
13.0%
Dispersal
In situ diversification
Migration into caves
Cave
Ancestors
Early adaptive population
Currently specialized species
De-evo
Ada-evo
Morph
Genet
Co-evo
Migration into caves
Bedrock
Vicariance
Precipitation (m/year)
2.2
1.8
1.4
8
4
0
-4
Deep ocean temperature (°C)
Eocene-Oligocene Climate Transition
Mid-Miocene Climatic Optimum (MMCO)
Crustal fracturing
Subsurface fissuring
Subterranean cave formation
In situ speciation emerged
Drip
CO₂
Water hole
Elevation (km)
6
5
4
3
2
1
0
QTP
Orogeny
Rapid elevation 25–15 Ma
Vicariance
Colonization
Introgression
Fragmented cave
Asian Monsoon Intensification
Subterranean cave isolation and connectivity
In situ speciation burst
River
CO₂
Drip
Eocene
Oligocene
Miocene
Pli.
Q.
40
30
20
10
0
Time before present (Ma)